Multiple ionization and x-ray line emission resulting from inner-shell electron ionization

V. L. Jacobs
E. O. Hulburt Center for Space Research, Naval Research Laboratory, Washington, D.C. 20375-5000

B. F. Rozsnyai
Lawrence Livermore National Laboratory, P.O. Box 808, Livermore, California 94550

(Received 31 January 1986)

We report an application of our previously developed model for determining the probabilities $P(\alpha_N, N_A)$ of emitting N_A Auger electrons and the probabilities $P(\alpha_N, \beta_N \rightarrow \gamma_N)$ of the radiative transitions $\beta_N \rightarrow \gamma_N$ during the cascade decay process following the creation of an arbitrary distribution α_N of N vacancies among the nl subshells of an atomic system. Particular emphasis has been given to the effects of single inner-shell vacancies, which may be created by energetic charged-particle collisions or by x-ray photoionization. Results of calculations are presented for single inner-shell electron ionization of iron ions from the neutral atom through the heliumlike ionization state, taking into account all of the Auger, Coster-Kronig, and electric dipole radiative transitions which can occur during the inner-shell vacancy-cascade process. The importance of the multiple ionization which results from Auger electron emission and of the x-ray satellite line radiation which is produced by the radiative decay of multiple-vacancy states is investigated for inner-shell electron ionization by electron collisions and by photon impacts.

I. INTRODUCTION

It is usually assumed that the thermal electron-collision processes which involve only the valence-shell electrons in multiply charged atomic ions play the dominant role in the excitation of the x-ray line emission spectra of high-temperature plasmas[1,2] and in the determination of the distribution of the various charge states due to ionization and recombination processes.[3,4] However, it has been pointed out that the high degree of ionization of iron ions which is produced in the gas surrounding galactic x-ray sources must be the result of Auger electron emission following the photoionization of a $1s$ inner-shell electron.[5,6] Moreover, the iron $K\alpha$ lines, which are produced by $1s \rightarrow 2p$ radiative transitions following the removal of a $1s$ inner-shell electron, are by far the most intense x-ray lines which are observed in the emission spectra of compact x-ray sources.[7] In this investigation we have developed a systematic procedure[8,9] for determining the probabilities of the single- and multiple-Auger-electron emissions as well as the probabilities for the various radiative transitions which can occur during the cascade decay of an arbitrary distribution of suddenly created atomic inner-shell vacancies. We present the results of calculations for the creation of the initial vacancy distribution by single inner-shell electron ionization of iron ions, which may be the result of charged-particle collisions or of photon impacts.

The ionization of an inner-shell electron may be followed by either a radiative transition or an Auger process. In either of these two alternative decay modes the initial inner-shell vacancy is transferred to a higher shell or subshell and additional inner-shell vacancies may be created. Further radiative or Auger transitions can then occur until the initial inner-shell vacancy and those subsequently created by Auger processes reach the outermost occupied shell. The result of this sequence of individual transitions, which has been called a vacancy cascade,[10] is the emission of many Auger electrons and/or photons. The K-shell electron ionization of a heavy atom can result in a very high degree of ionization. In addition, the characteristic x-ray emission lines, which are identified with the radiative transitions that fill the initial single inner-shell vacancy, can be accompanied by prominent satellite lines, which are associated with the corresponding radiative transitions from multiple-vacancy states produced by Auger processes.

In this investigation, we have employed our previously developed comprehensive description[8,9] of the atomic rearrangement process, in which the equilibrium populations are determined for all of the single- and multiple-vacancy states which can be formed during the cascade decay of a suddenly created initial vacancy distribution. Calculations have been previously presented for neutral iron atoms.[8,9] We now report the extension of our calculations to the various states of ionization, with particular emphasis being given to the effects of the energetic closing of the channels for certain Auger transitions on the vacancy distributions and on the fluorescence yields. For completeness our general procedure is reviewed in Sec. II, where the cross sections for single and multiple ionization as well as for x-ray line and satellite emission are defined in terms of the equilibrium populations of the vacancy states. Our method is a natural extension of the procedure employed by Weisheit,[6] in that we have systematically taken into account all allowed radiative and Auger transitions and have not been inhibited by the necessity of predetermining the most probable decay processes. In our

general formalism we have also allowed for the creation of an arbitrary distribution of initial vacancies. Our vacancy-cascade model is comparable in its sophistication to the procedure developed by Carlson and Krause,[11,12] but they have employed random selection techniques in order to reduce the very large number of decay sequences which may be involved in the creation of a given final charge state. All possible decay sequences have been systematically taken into account in our calculations, which are described in Sec. III for the single- and multiple-ionization probabilities as well as for the line and satellite emission probabilities resulting from the cascade decay of the single inner-shell vacancies which can be created in the various *nl* subshells of iron ions. In Sec. IV, we treat single inner-shell electron ionization by electron collisions and by photon impacts. Our conclusions are presented in Sec. V.

II. THE VACANCY-CASCADE MODEL

We denote by α_N a distribution of N vacancies among the occupied *nl* subshells of an atomic system. For example, $1s\,2s^2 2p^6$ would represent a distribution with a single K-shell vacancy in the neonlike ion Fe XVII ($N=1$), $1s^2 2s^2 2p^5$ would represent a distribution that could be formed from the initial distribution by a radiative transition ($N=1$), and $1s^2 2s\,2p^5$ would represent a distribution that could be the result of an Auger process ($N=2$). In the application to heavier atomic systems for which relativistic corrections are important, it would be necessary to employ the j representation for the specification of the single-electron vacancy states. In order to take into account the enormous number of elementary radiative and Auger transitions which can occur in the vacancy-cascade process, it has been necessary to utilize atomic transition rates which have been averaged over the LS and J substates of the atomic eigenstates.

We shall assume that the vacancy decay processes are independent of the mechanism by which the initial vacancy distribution is created. In a rigorous quantum-electrodynamical description of the complete collision process,[13] it would be necessary to evaluate the resonant multichannel scattering matrix by introducing intermediate Fock-space states which consist of the inner-shell vacancy distributions combined with the states of all emitted and scattered electrons and/or photons. The total spontaneous decay rate $\Gamma(\alpha_N)$ of the vacancy distribution α_N can be defined by

$$\Gamma(\alpha_N)=\sum_{\beta_N} A_r(\alpha_N\rightarrow\beta_N)+\sum_{\gamma_{N+1}} A_A(\alpha_N\rightarrow\gamma_{N+1})\ , \tag{1}$$

where $A_r(\alpha_N\rightarrow\beta_N)$ denotes the rate for the radiative transition to the N-vacancy state β_N and $A_A(\alpha_N\rightarrow\gamma_{N+1})$ is the rate for the Auger transition to the $(N+1)$-vacancy state γ_{N+1}. If full account could be taken of the interaction between the atomic system and the quantized radiation field,[14–16] the relative probabilities for decay into the various electron- and photon-continuum channels would be altered by the electromagnetic coupling between the unperturbed final continuum states which are the result of the first-order autoionization and radiative decay processes.

We will take into account all single-photon emission processes which correspond to a single-electron electric-dipole transition and all autoionization processes which result in the creation of one additional vacancy and in the emission of a single Auger electron. In our calculations we have neglected core relaxation and configuration interaction. The inclusion of these corrections would give rise to nonvanishing transition rates for simultaneous multiple emission processes, as has been demonstrated by Aberg.[17]

We consider a statistical ensemble of identical atomic systems in which the vacancy distribution α_N is continuously created at a rate per unit volume $R_i(\alpha_N)$ during the initial collisional ionization or photoionization process. The complete set of population densities $M(\alpha_N)$, which describes the steady-state balance between all vacancy creation and decay processes, can be obtained by solving the set of equations

$$R_i(\alpha_N)+\sum_{\beta_N} M(\beta_N)A_r(\beta_N\rightarrow\alpha_N)+\sum_{\gamma_{N-1}} M(\gamma_{N-1})A_A(\gamma_{N-1}\rightarrow\alpha_N)=M(\alpha_N)\Gamma(\alpha_N)\ . \tag{2}$$

Note that a given distribution of vacancies α_N may be created in three separate ways, by the initial ionization mechanism, by a radiative transition from another distribution of N vacancies β_N, or by an Auger process from a distribution of $N-1$ vacancies γ_{N-1}.

The multiple-ionization and x-ray line emission cross sections may be conveniently defined in terms of the populations $\rho(\alpha_N)$ of the vacancy states α_N per unit current density J_i of the incident charged particles or photons. The populations per unit current density $\rho(\alpha_N)$ are related to the population densities $M(\alpha_N)$ according to

$$\rho(\alpha_N)=\frac{M(\alpha_N)}{M_T J_i}\ , \tag{3}$$

where M_T denotes the total number of atomic systems (Fe nuclei in the present investigation) per unit volume. If we specify by Ω_N the outer-shell N-vacancy states from which further Auger transitions cannot occur, the total N-electron loss or N-fold ionization cross section can be defined by

$$\sigma_L(N)=\sum_{\Omega_N}\left[\sigma_i(\Omega_N)+\sum_{\alpha_N}\rho(\alpha_N)A_r(\alpha_N\rightarrow\Omega_N)+\sum_{\gamma_{N-1}}\rho(\gamma_{N-1})A_A(\gamma_{N-1}\rightarrow\Omega_N)\right]\ , \tag{4}$$

where $\sigma_i(\Omega_N)$ are the cross sections for the simultaneous initial ionization of N outer-shell electrons, the second term corresponds to the contribution resulting from radiative transitions from the inner-shell N-vacancy states α_N, and the last term represents the contribution of Auger transitions from the inner-shell $(N-1)$-vacancy states γ_{N-1}. The simultaneous initial multiple-ionization pro-

cess has been ignored in the calculations reported in the present investigation. In other words, $\sigma_i(\Omega_N)$ is to be replaced by $\delta(N,1)\delta(\Omega_N,n_il_i)$. This is expected to be a good approximation in the case of photoionization.

The cross section describing the emission of x-ray line radiation in the transition $\alpha_N \rightarrow \beta_N$ can be simply defined in terms of the population densities $\rho(\alpha_N)$ by

$$\sigma_r(\alpha_N \rightarrow \beta_N) = \rho(\alpha_N) A_r(\alpha_N \rightarrow \beta_N) \ . \tag{5}$$

If we neglect the radiative rearrangement of the N-vacancy distribution α_N, which is taken into account by including the second term on the left-hand side of Eq. (2), Eq. (5) can be reduced to the familiar product of an effective vacancy production cross section and the conventional fluorescence yield $A_r(\alpha_N \rightarrow \beta_N)/\Gamma(\alpha_N)$. In high-$Z$ atomic systems, where the K-shell radiative transition rates are relatively large, it becomes necessary to employ the more general description of the production of radiative emission which takes into account this radiative rearrangement. The radiative decays of multiple-vacancy ($N > 1$) states which have been formed by Auger processes produce satellite lines that usually occur on the short-wavelength side of the characteristic x-ray lines, which are associated with the corresponding radiative transitions from single-vacancy ($N = 1$) states. It is clear that the spectral feature which is experimentally identified as the characteristic x-ray line may contain a significant intensity contribution from unresolvable satellite lines.

III. MULTIPLE-IONIZATION AND X-RAY EMISSION PROBABILITIES RESULTING FROM SINGLE-n-VACANCY CREATION IN IRON IONS

We now describe the application of our vacancy-cascade model to evaluate the multiple-ionization and x-ray emission probabilities resulting from the cascade decay of the single inner-shell vacancies which can be created in the various nl subshells of iron ions. Initial multiple ionization will therefore be neglected. It should be emphasized that our treatment of the atomic rearrangement process as a vacancy cascade is based on the assumption that the vacancy creation and decay processes can be treated as independent events.

The effects of a single vacancy in the nl subshell can be investigated by replacing the initial vacancy production cross section $\sigma_i(\alpha_N)$ by $\delta(N,1)\delta(\alpha_N,nl)$. Equations (4) and (5) will then define dimensionless quantities which can be interpreted, respectively, as the probabilities for the multiple ionization and the x-ray emission which will result from the cascade decay of a single nl-subshell vacan-

TABLE I. Fluorescence probabilities $P^{(N)}(nl,n_1n_1 \rightarrow n_2l_2)$ for the $n_1l_1 \rightarrow n_2l_2$ characteristic line emissions from single-vacancy states ($N=1$) formed by the creation of a single nl inner-shell vacancy in neutral iron (Fe I) and in the iron ions Fe II–Fe VIII. (Numbers in square brackets are powers of ten.)

$n_1l_1 \rightarrow n_2l_2$	Fe I	Fe II	Fe III	Fe IV	Fe V	Fe VI	Fe VII	Fe VIII
				$nl = 1s$				
$1s \rightarrow 2p$	0.28	0.29	0.29	0.28	0.28	0.27	0.27	0.26
$1s \rightarrow 3p$	0.34[−1]	0.34[−1]	0.35[−1]	0.36[−1]	0.37[−1]	0.39[−1]	0.40[−1]	0.40[−1]
$2s \rightarrow 2p$								
$2s \rightarrow 3p$								
$2p \rightarrow 3s$	0.13[−3]	0.15[−3]	0.15[−3]	0.15[−3]	0.16[−3]	0.17[−3]	0.19[−3]	0.19[−3]
$2p \rightarrow 3d$	0.18[−2]	0.18[−2]	0.18[−2]	0.17[−2]	0.15[−2]	0.12[−2]	0.96[−3]	0.51[−3]
$3s \rightarrow 3p$	0.68[−9]	0.96[−9]	0.22[−7]	0.34[−7]	0.62[−7]			
$3p \rightarrow 3d$	0.77[−6]	0.89[−6]	0.11[−5]					
				$nl = 2s$				
$2s \rightarrow 2p$	0.57[−5]	0.63[−5]	0.77[−5]	0.81[−5]	0.22[−4]	0.27[−4]	0.17[−3]	0.19[−3]
$2s \rightarrow 3p$	0.27[−3]	0.29[−3]	0.37[−3]	0.40[−3]	0.11[−2]	0.15[−2]	0.10[−1]	0.11[−1]
$2p \rightarrow 3s$	0.26[−8]	0.32[−8]	0.41[−8]	0.44[−8]	0.12[−7]	0.17[−7]	0.12[−6]	0.16[−6]
$2p \rightarrow 3d$	0.36[−7]	0.40[−7]	0.48[−7]	0.48[−7]	0.11[−6]	0.12[−6]	0.62[−6]	0.36[−6]
$3s \rightarrow 3p$	0.14[−13]	0.21[−13]	0.59[−12]	0.98[−12]	0.48[−11]			
$3p \rightarrow 3d$	0.62[−8]	0.76[−8]	0.11[−7]					
				$nl = 2p$				
$2p \rightarrow 3s$	0.46[−3]	0.53[−3]	0.53[−3]	0.55[−3]	0.57[−3]	0.61[−3]	0.69[−3]	0.79[−3]
$2p \rightarrow 3d$	0.64[−2]	0.64[−2]	0.62[−2]	0.59[−2]	0.53[−2]	0.45[−2]	0.35[−2]	0.19[−2]
$3s \rightarrow 3p$	0.24[−8]	0.33[−8]	0.76[−7]	0.12[−6]	0.22[−8]			
$3p \rightarrow 3d$	0.55[−13]	0.86[−13]	0.23[−11]					
				$nl = 3s$				
$3s \rightarrow 3p$	0.53[−5]	0.64[−5]	0.15[−3]	0.22[−3]	0.39[−3]			
$3p \rightarrow 3d$	0.12[−9]	0.17[−9]	0.43[−8]					
				$nl = 3p$				
$3p \rightarrow 3d$	0.24[−4]	0.26[−4]	0.30[−4]					

TABLE II. Fluorescence probabilities $P^{(N)}(nl,n_1l_1\rightarrow n_2l_2)$ for the $n_1l_1\rightarrow n_2l_2$ characteristic line emissions from single-vacancy states ($N=1$) formed by the creation of a single nl inner-shell vacancy in the iron ions Fe IX–Fe XXIV. (Numbers in square brackets are powers of ten.)

$n_1l_1\rightarrow n_2l_2$	Fe IX	Fe X	Fe XI	Fe XII	Fe XIII	Fe XIV	Fe XV	Fe XVI
				$nl=1s$				
$1s\rightarrow 2p$	0.26	0.27	0.29	0.30	0.32	0.34	0.37	0.38
$1s\rightarrow 3p$	0.42[−1]	0.38[−1]	0.33[−1]	0.27[−1]	0.20[−1]	0.11[−1]		
$2p\rightarrow 3s$	0.23[−3]	0.32[−3]	0.47[−3]	0.77[−3]	0.15[−2]	0.49[−2]	0.23[−1]	0.38
				$nl=2s$				
$2s\rightarrow 2p$	0.23[−3]	0.24[−3]	0.27[−3]	0.32[−3]	0.40[−3]	0.55[−3]	0.10[−2]	
$2s\rightarrow 3p$	0.15[−1]	0.15[−1]	0.14[−1]	0.13[−1]	0.12[−1]	0.91[−2]		
$2p\rightarrow 3s$	0.20[−6]	0.28[−6]	0.45[−6]	0.86[−6]	0.18[−5]	0.80[−5]	0.64[−4]	
				$nl=2p$				
$2p\rightarrow 3s$	0.88[−3]	0.12[−2]	0.17[−2]	0.26[−2]	0.46[−2]	0.14[−1]	0.62[−1]	
$n_1l_1\rightarrow n_2l_2$	Fe XVII	Fe XVIII	Fe XIV	Fe XX	Fe XXI	Fe XXII	Fe XXIII	Fe XXIV
$1s\rightarrow 2p$	0.39	0.41	0.43	0.46	0.48	0.49		

cy. The equilibrium populations of all single- and multiple-vacancy states can now be determined by the application of our vacancy-cascade model, which incorporates the radiative rearrangement of the initial vacancy distribution as well as of all multiple-vacancy distributions that can be subsequently created by Auger processes.

The first-order nonrelativistic perturbation-theory expressions for the radiative and Auger transition rates from single-vacancy states in the various ions of iron have been evaluated in the frozen-core approximation, using wave functions obtained from a Hartree-Slater self-consistent-field model.[9] The creation of multiple vacancies in these ions causes shifts in the emitted photon frequencies and may result in an energetic closing of the channels for certain Coster-Kronig transitions, which are Auger transitions involving vacancy transfer within a given n shell. In the determination of the population densities of the multiple-vacancy states, we have not attempted to correct the radiative or Auger transition rates for these effects. The incorporation of these corrections to the transition energies as well as of other departures from the frozen-core approximation would involve an enormous increase in our computational effort. However, the multiple-vacancy radiative and Auger transition rates have been systematically corrected, as described previously,[8] to take into account the number of electrons remaining in the relevant nl subshells following one or more Auger transitions.

The replacement of the initial vacancy production cross section $\sigma_i(\alpha_N)$ by $\delta(N,1)\delta(\alpha_N,nl)$ converts the x-ray emission cross section defined by Eq. (5) into the probability $P^{(N)}(nl,n_1l_1\rightarrow n_2l_2)$ that the creation of a single nl-subshell vacancy will give rise to photon emission through the transition $n_1l_1\rightarrow n_2l_2$ in a state consisting of N vacancies during the cascade decay process. The complete set of fluorescence probabilities $P^{(N)}(nl,n_1\rightarrow n_2l_2)$ clearly provides a more comprehensive description of the photon emission spectrum than the conventional fluorescence yields $P^{(1)}(nl,nl\rightarrow n_2l_2)$, which refer only to characteristic line emission ($N=1$) from the initial vacancy state ($n_1l_1=nl$) and usually are not corrected for the effects of the vacancy transfers that result from radiative processes.

In Tables I and II we present for each initial nl-subshell vacancy our results for the fluorescence probabilities $P^{(1)}(nl,n_1l_1\rightarrow n_2l_2)$ which describe the emission of the

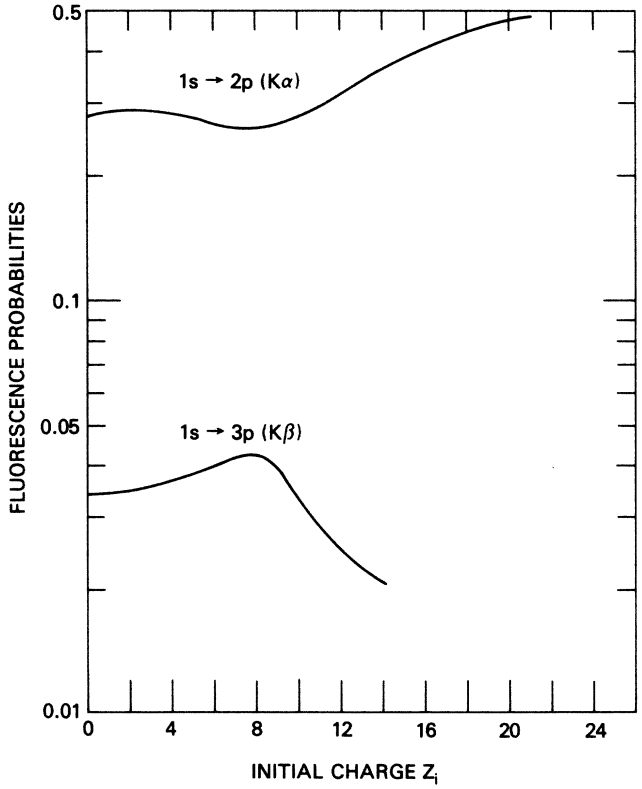

FIG. 1. The fluorescence probabilities $P^{(1)}(1s,1s\rightarrow 2p)$ and $P^{(1)}(1s,1s\rightarrow 3p)$ describing the characteristic line emissions $1s\rightarrow 2p$ ($K\alpha$) and $1s\rightarrow 3p$ ($K\beta$) during the cascade decay process following the creation of a single $1s$ vacancy in iron ions with initial charge Z_i.

TABLE III. Fluorescence probabilities $P^{(N)}(nl,n_1l_1\rightarrow n_2l_2)$ for the $n_1l_1\rightarrow n_2l_2$ satellite line emissions from multiple-vacancy states ($N>1$) formed by the creation of a single nl inner-shell vacancy in neutral iron (Fe I) and in the iron ions Fe II–Fe VIII. (Numbers in square brackets are powers of ten.)

$n_1l_1\rightarrow n_2l_2$	Fe I	Fe II	Fe III	Fe IV	Fe V	Fe VI	Fe VII	Fe VIII
				$nl=1s$				
$2s\rightarrow 2p$	0.11[−5]	0.13[−5]	0.16[−5]	0.17[−5]	0.46[−5]	0.58[5]	0.54[−5]	0.62[−4]
$2s\rightarrow 3p$	0.59[−4]	0.68[−4]	0.83[−4]	0.90[−4]	0.26[−3]	0.34[−3]	0.30[−2]	0.36[−2]
$2p\rightarrow 3s$	0.60[−3]	0.68[−3]	0.70[−3]	0.76[−3]	0.77[−3]	0.82[−3]	0.75[−3]	0.83[−3]
$2p\rightarrow 3d$	0.62[−2]	0.60[−2]	0.66[−2]	0.77[−2]	0.64[−2]	0.55[−2]	0.39[−2]	0.23[−2]
$3s\rightarrow 3p$	0.20[−5]	0.27[−5]	0.40[−5]	0.21[−5]	0.23[−5]	0.10[−4]	0.19[−4]	0.20[−4]
$3p\rightarrow 3d$	0.66[−4]	0.93[−4]	0.94[−4]	0.63[−3]	0.65[−3]	0.55[−4]	0.39[−4]	0.21[−4]
				$nl=2s$				
$2p\rightarrow 3s$	0.52[−3]	0.60[−3]	0.60[−3]	0.63[−5]	0.58[−3]	0.60[−3]		
$2p\rightarrow 3d$	0.58[−2]	0.57[−2]	0.54[−2]	0.62[−2]	0.39[−2]	0.29[−2]		
$3s\rightarrow 3p$	0.26[−5]	0.34[−5]	0.26[−3]	0.62[−3]	0.83[−2]			
$3p\rightarrow 3d$	0.72[−4]	0.11[−3]	0.11[−3]	0.17[−3]	0.14[−3]			
				$nl=2p$				
$3s\rightarrow 3p$	0.88[−6]	0.11[−5]	0.52[−4]	0.35[−4]	0.76[−4]			
$3p\rightarrow 3d$	0.34[−4]	0.43[−4]	0.45[−4]	0.52[−4]	0.78[−4]			
				$nl=3s$				
$3p\rightarrow 3d$	0.25[−4]	0.29[−4]						

various characteristic lines $n_1l_1\rightarrow n_2l_2$ in neutral iron and in iron ions. The fluorescence probabilities $P^{(1)}(1s,1s\rightarrow 2p)$ and $P^{(1)}(1s,1s\rightarrow 3p)$ for Fe I are in close agreement, respectively, with the $K\alpha$ and $K\beta$ fluorescence yields given by Bambynek *et al.*,[18] and the L-shell fluorescence yields are also in good agreement. The variations of the $1s\rightarrow 2p$ ($K\alpha$) and $1s\rightarrow 3p$ ($K\beta$) fluorescence probabilities with the degree of ionization of the initial iron ion are illustrated in Fig. 1.

The satellite emission probabilities $P^{(N)}(nl,n_1l_1\rightarrow n_2l_2)$ ($N>1$) for each initial nl-subshell vacancy are presented in Tables III and IV. The satellite distributions have not been subdivided into the separate contributions resulting from double ($N=2$), triple ($N=3$), and higher states of ionization even though these separate contributions can be identified in our calculations. In addition, no attempt has been made to distinguish between resolvable and unresolvable satellite lines since this distinction depends upon the spectral resolution of the particular observation. The emission of satellite radiation following one or more Auger processes is predicted to be more probable for iron than the excitation of the corresponding characteristic lines by the transfer of the initial vacancy due to radiative processes. For an initial $2s$-subshell ($L_{\rm I}$) vacancy in Fe I–Fe VI, the most probable photon-emission process is found to be the $2p\rightarrow 3d$ ($L\alpha$) satellite emission following a $2s\rightarrow 2p\,3d$ ($L_{\rm I}\rightarrow L_{\rm II,III}M_{\rm IV,V}$) Coster-Kronig transition.

The replacement of the initial vacancy production cross section $\sigma_i(\alpha_N)$ by $\delta(N,1)\delta(\alpha_N,nl)$ transforms Eq. (4) into the definition of the probability $P(nl,N_A)$ that the creation of a single nl-subshell vacancy will result in the ejection of N_A Auger electrons during the cascade decay process. If the initially ionized nl electron is taken into account, the total number of ejected electrons N_e is given by

$$N_e=N_A+1\ . \tag{6}$$

The probabilities $P(nl,N_A)$ for an ion whose initial charge is Z_i before ionization can be interpreted as the fractional abundances of the various final ionic products with charges

$$Z_f=N_e+Z_i\ . \tag{7}$$

The single- and multiple-ionization probabilities resulting from the cascade decay of single inner-shell vacancies in neutral iron and in iron ions are presented in Tables V and VI. It is found that the cascade decay process following the creation of a single K-shell vacancy can result in the emission of as many as $N_A=8$ Auger electrons. It is also

TABLE IV. Fluorescence probabilities $P^{(N)}(nl,n_1l_1\rightarrow n_2l_2)$ for the $n_1l_1\rightarrow n_2l_2$ satellite line emissions from multiple-vacancy states ($N>1$) formed by the creation of a single nl inner-shell vacancy in the iron ions Fe IX–Fe VVI. (Numbers in square brackets are powers of ten.)

$n_1l_1\rightarrow n_2l_2$	Fe IX	Fe X	Fe XI	Fe XII	Fe XIII	Fe XIV	Fe XV	Fe XVI
				$nl=1s$				
$2s\rightarrow 2p$	0.91[−4]	0.11[−3]	0.16[−3]	0.25[−3]	0.48[−3]	0.16[−3]		
$2s\rightarrow 3p$	0.56[−2]	0.63[−2]	0.73[−2]	0.92[−2]	0.13[−1]	0.28[−2]		
$2p\rightarrow 3s$	0.10[−2]	0.15[−2]	0.24[−2]	0.49[−2]	0.16[−1]	0.98[−2]		
$3s\rightarrow 3p$	0.35[−4]	0.42[−4]	0.54[−4]	0.74[−4]	0.14[−3]	0.11[−4]		

TABLE V. Probabilities $P(nl,N_A)$ for the emission of N_A Auger electrons following the creation of a single nl inner-shell vacancy in neutral iron (Fe I) and in the iron ions Fe II–Fe VIII. (Numbers in square brackets are powers of ten.)

N_A	Fe I	Fe II	Fe III	Fe IV	Fe V	Fe VI	Fe VII	Fe VIII
				$nl=1s$				
0	0.18[−2]	0.18[−2]	0.18[−2]	0.38[−1]	0.39[−1]	0.41[−1]	0.41[−1]	0.41[−1]
1	0.90[−1]	0.86[−1]	0.83[−1]	0.24	0.24	0.28	0.28	0.27
2	0.96[−1]	0.99[−1]	0.97[−1]	0.21	0.22	0.23	0.28	0.29
3	0.14	0.13	0.18	0.26	0.25	0.34	0.40	0.40
4	0.13	0.13	0.88[−1]	0.18	0.19	0.90[−1]		
5	0.15	0.15	0.41	0.61[−1]	0.61[−1]	0.19[−1]		
6	0.13	0.34	0.34[−1]	0.12[−1]	0.56[−2]			
7+8	0.26	0.6[−1]	0.11					
				$nl=2s$				
0	0.42[−7]	0.48[−7]	0.59[−7]	0.40[−3]	0.11[−2]	0.15[−2]	0.10[−1]	0.10[−1]
1	0.67[−2]	0.59[−2]	0.68[−2]	0.14[−1]	0.21[−1]	0.17	0.99	0.99
2	0.62[−1]	0.51[−1]	0.75[−1]	0.82	0.80	0.83		
3	0.19	0.18	0.20	0.16	0.18			
4	0.30	0.29	0.38	0.89[−2]				
5	0.27	0.29	0.34					
6	0.14	0.19						
7	0.10							
				$nl=2p$				
0	0.64[−2]	0.64[−2]	0.62[−2]	0.59[−2]	0.53[−2]	0.51[−2]	0.42[−2]	0.27[−2]
1	0.20	0.18	0.17	0.84	0.82	0.99	0.99	0.99
2	0.33	0.33	0.33	0.15	0.16			
3	0.33	0.35	0.50	0.78[−2]	0.82[−2]			
4	0.12	0.13						
				$nl=3s$				
0	0.12[−9]	0.17[−9]	0.43[−8]	0.22[−3]	0.39[−3]	1.00	1.00	
1	0.67[−1]	0.62[−1]	0.10[1]	0.10[1]	0.10[1]			
2	0.93	0.94						
				$nl=3p$				
0	0.00	0.00	0.00	1.00	1.00	1.00	1.00	
1	1.00	1.00	1.00					

TABLE VI. Probabilities $P(nl,N_A)$ for the emission of N_A Auger electrons following the creation of a single nl inner-shell vacancy in the iron ions Fe IX–Fe XXIV. (Numbers in square brackets are powers of ten.)

N_A	Fe IX	Fe X	Fe XI	Fe XII	Fe XIII	Fe XIV	Fe XV	Fe XVI
				$nl=1s$				
0	0.43[−1]	0.39[−1]	0.33[−1]	0.28[−1]	0.21[−1]	0.16[−1]	0.23[−1]	0.38
1	0.27	0.28	0.29	0.31	0.32	0.34	0.35	0.62
2	0.29	0.27	0.25	0.22	0.20	0.64	0.63	
3	0.39	0.41	0.43	0.44	0.46			
				$nl=2s$				
0	0.15[−1]	0.15[−1]	0.14[−1]	0.13[−1]	0.12[−1]	0.91[−1]	0.64[−1]	1.00
1	0.99	0.99	0.99	0.99	0.99	0.99	1.00	
				$nl=2p$				
0	0.88[−3]	0.12[−2]	0.17[−2]	0.26[−2]	0.46[−2]	0.14[−1]	0.62[−1]	1.00
1	0.99	0.99	0.99	0.99	0.99	0.99	0.94	

N_A	Fe XVII	Fe XVIII	Fe XIX	Fe XX	Fe XXI	Fe XXII	Fe XXIII	Fe XXIV
				$nl=1s$				
0	0.39	0.41	0.43	0.46	0.48	0.49	0.00	1.00
1	0.61	0.59	0.57	0.54	0.52	0.51	1.00	

noted that for single $3p$-subshell ($M_{II,III}$) vacancy creation in Fe I–Fe III the double-ionization process occurs with almost unit probability due to the very large rates for the $3p \rightarrow 3d^2$ Coster-Kronig transitions.

In Fig. 2 we present as functions of the initial charge Z_i the mean final charges $\langle Z_f \rangle$ resulting from the cascade decay of the single inner-shell vacancies which can be created in the various nl subshells of iron ions. Because of the property that the ionization probabilities $P(nl,N_A)$ corresponding to each initial nl-subshell vacancy are normalized to unity, the mean final charges $\langle Z_f \rangle$ may be obtained from the relationship

$$\langle Z_f \rangle = \sum_{Z_f} Z_f \delta(Z_f, Z_i + N_A + 1) P(nl, N_A) . \quad (8)$$

As anticipated, the mean final charge is found to increase with increasing binding energy of the subshell in which the initial vacancy is created. The only exception to this trend occurs in the creation of a single K-shell vacancy in Fe I–Fe II, which gives rise to a lower mean final charge than a L_I-subshell vacancy. This exception can be attributed to the large rates for the $1s \rightarrow np$ radiative transitions, which transfer the initial K-shell vacancy to the $2p$ ($L_{II,III}$) and $3p$ ($M_{II,III}$) subshells without further ionization, and to the fact that Auger processes from the $2p$ ($L_{II,III}$) subshell have larger rates than the K-shell Auger processes. The sharp discontinuities in Fig. 2 are consequences of the energetic closing of the channels for the L- and M-shell Coster-Kronig transitions. Analogous effects appear in some of the fluorescence probabilities. A detailed discussion of this phenomenon has been previously presented.[9]

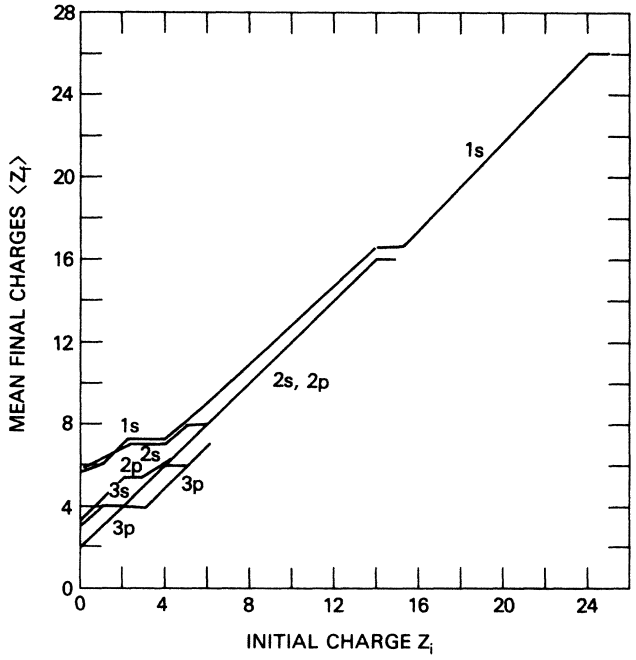

FIG. 2. The mean final charges $\langle Z_f \rangle$ resulting from the cascade decay of single inner-shell vacancies which can be created in the various nl subshells of iron ions with initial charge Z_i.

IV. SINGLE INNER-SHELL ELECTRON IONIZATION BY ELECTRON COLLISIONS AND BY PHOTON IMPACTS

The cross sections describing multiple ionization and photon emission can be evaluated by combining the nl-subshell probabilities which have been presented in Sec. III with the corresponding single inner-shell electron ionization cross sections. The nl-subshell cross sections for electron-collisional ionization have been calculated by Moores, Golden, and Sampson[19] and have been presented by them in the convenient parametrized form

$$\sigma_e(nl) = \pi a_0^2 \left[\frac{E_H}{E_{nl}}\right]^2 \left[\frac{N_{nl}}{u}\right] \times \left[A(nl)\ln(u) + D(nl)\left[1-\frac{1}{u}\right]^2 + \frac{c(nl)}{u} + \frac{d(nl)}{u^2}\left[1-\frac{1}{u}\right]\right], \quad (9)$$

where u is the incident electron energy measured in units of the nl-subshell ionization threshold energy E_{nl} and N_{nl} is the number of nl-subshell electrons. The remaining

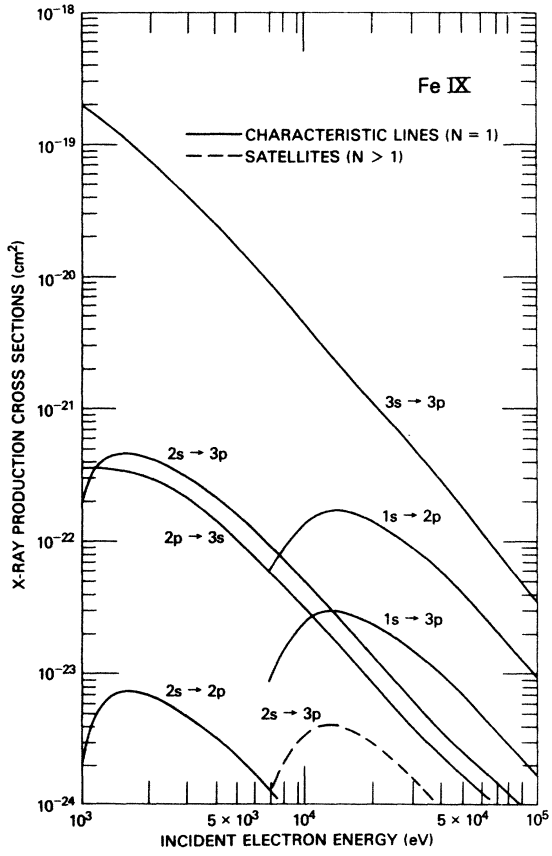

FIG. 3. The cross sections $\sigma_r^{(N)}(n_1 l_1 \rightarrow n_2 l_2)$ for the radiative emissions $n_1 l_1 \rightarrow n_2 l_2$ during the vacancy-cascade decay process following single-electron ionization from the various nl subshells of argonlike Fe IX ions by electron collisions, obtained from the evaluation of Eq. (11).

symbols have their conventional meaning. This representation of the subshell cross sections exhibits the well-known property[20] that the electron-collisional ionization of the most loosely bound valence-shell electrons is dominant over inner-shell electron ionization for all values of the incident electron energy.

The nl-subshell photoionization cross sections for neutral iron and for iron ions have been calculated using a Hartree-Slater self-consistent-field model.[21] The relative importance of the individual nl-subshell cross sections, for a particular value of the incident photon energy $\hbar\omega$, can be anticipated from the properties of the hydrogenic cross section:

$$\sigma_p(nl)=\frac{64\pi\alpha a_0^2}{3^{3/2}}\left[\frac{N_{nl}}{2l+1}\right]\left[\frac{E_H}{\hbar\omega}\right]^3\left[\frac{Z^4}{n^3}\right]g(nl)\ . \tag{10}$$

The Gaunt factor $g(nl)$ is close to unity at the ionization threshold and decreases asymptotically as $(\hbar\omega)^{-0.5-l}$. It can be seen that photoionization from the most tightly bound nl subshell that can be ionized, at the given incident photon energy, will be more probable than photoionization from the higher-n shells and that for a particular value of n the lowest values of l will have the largest asymptotic cross section. This behavior of the subshell photoionization cross sections is indeed exhibited by the nonhydrogenic results and is in marked contrast with the variation of the subshell cross sections for electron-collisional ionization.

The cross section $\sigma_r^{(N)}(n_1l_1\rightarrow n_2l_2)$ describing the emission of line radiation in the transition $n_1l_1\rightarrow n_2l_2$ from an N-vacancy state can be evaluated by combining the individual single inner-shell vacancy creation cross sections $\sigma(nl)$ with the fluorescence probabilities $P^{(N)}(nl,n_1l_1\rightarrow n_2l_2)$ according to the relationship

$$\sigma_r^{(N)}(n_1l_1\rightarrow n_2l_2)=\sum_{nl}P^{(N)}(nl,n_1l_1\rightarrow n_2l_2)\sigma(nl)\ . \tag{11}$$

The cross sections for the production of the most intense radiative emissions by electron-collisional ionization are illustrated for the representative cases of argonlike Fe IX and neonlike Fe XVII ions in Figs. 3 and 4, and the corresponding results which we have obtained for photoionization are displayed in Figs. 5 and 6. The total satellite contribution ($N>1$) associated with a given characteristic line ($N=1$) is represented by a dashed curve. The neglect of initial double K-shell ionization accounts for the absence of any prediction for $1s\rightarrow np$ K-shell satellite radiation. As anticipated, the $2p\rightarrow 3d$ ($L\alpha$) characteristic line

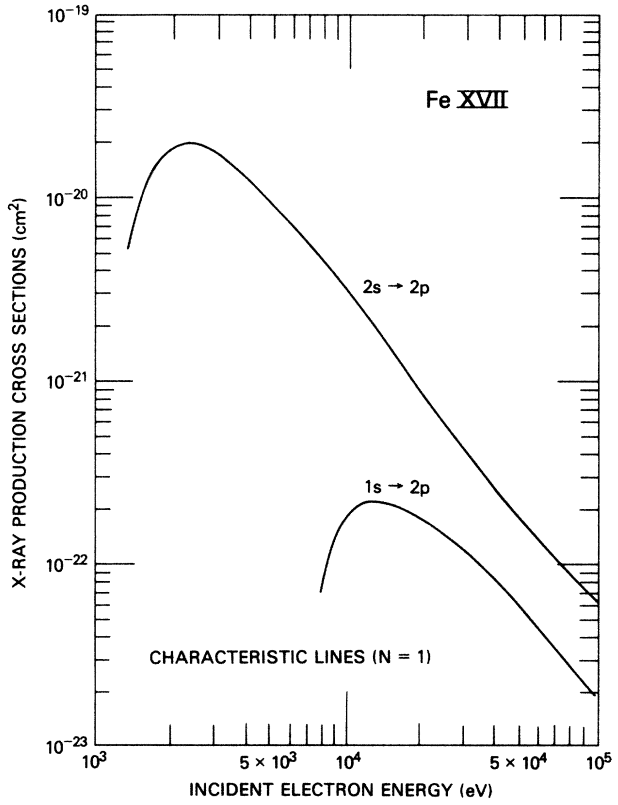

FIG. 4. The cross sections $\sigma_r^{(N)}(n_1l_1\rightarrow n_2l_2)$ for the radiative emissions $n_1l_1\rightarrow n_2l_2$ during the vacancy-cascade decay process following single-electron ionization from the various nl subshells of neonlike Fe XVII ions by electron collisions, obtained from the evaluation of Eq. (11).

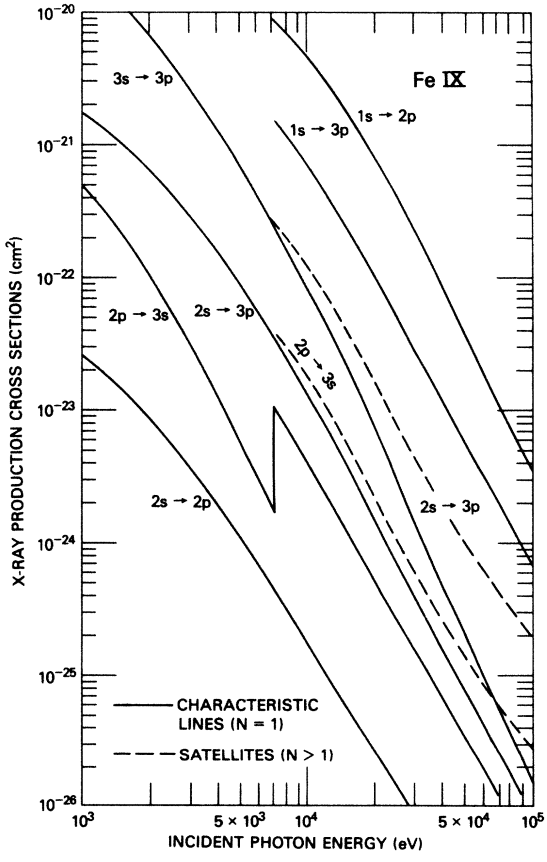

FIG. 5. The cross sections $\sigma_r^{(N)}(n_1l_1\rightarrow n_2l_2)$ for the radiative emissions $n_1l_1\rightarrow n_2l_2$ during the vacancy-cascade decay process following single-electron photoionization from the various nl subshells of argonlike Fe IX ions, obtained from the evaluation of Eq. (11).

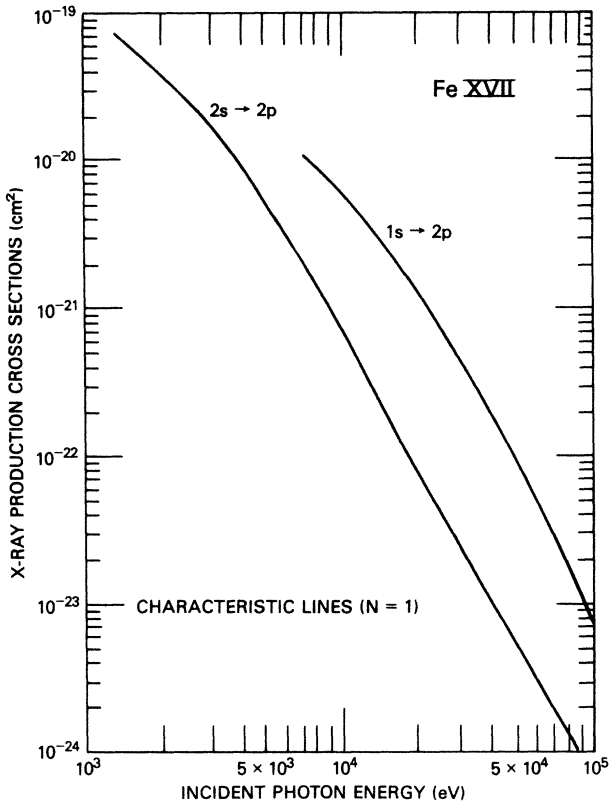

FIG. 6. The cross sections $\sigma_r^{(N)}(n_1l_1 \rightarrow n_2l_2)$ for the radiative emissions $n_1l_1 \rightarrow n_2l_2$ during the vacancy-cascade decay process following single-electron photoionization from the various nl subshells of neonlike Fe XVII ions, obtained from the evaluation of Eq. (11).

emission is predicted to be the most intense radiative transition during the cascade decay process following single inner-shell vacancy creation in the ions Fe II–Fe VIII, except at incident energies which are sufficiently high for the K-shell lines to be dominant. This is illustrated for neutral iron atoms in Fig. 8 of our previously reported investigation.[8]

The ratio of the satellite intensity relative to the corresponding characteristic line intensity is significantly affected by the different incident-energy behaviors of the electron-collisional ionization and photoionization cross sections $\sigma_e(nl)$ and $\sigma_p(nl)$. For incident energies below the K-shell ionization threshold, the $2p \rightarrow 3p$ ($L\alpha$) satellite emission in the ions Fe II–Fe VIII can be produced only by means of the $2s \rightarrow 2p\,3l$ ($L_{\rm I} \rightarrow L_{\rm II,III}M$) Coster-Kronig transitions following $2s$-subshell ionization, and the $L\alpha$ satellite intensity is found to be less than the characteristic line intensity for both of the two ionization mechanisms. Above the K-shell ionization threshold, however, the additional Auger processes which can occur are found to produce an order-of-magnitude enhancement in the relative $L\alpha$ satellite line intensity during the cascade process following inner-shell electron photoionization. An analogous result has been predicted in our earlier investigation for neutral iron atoms.[8] The results obtained for the photoionization of argonlike Fe IX ions, which are illustrated in Fig. 5, show an analogous enhancement of the $2s \rightarrow 3p$ and $2p \rightarrow 3s$ satellite emissions, which become dominant over the respective characteristic line emissions above the K-shell ionization threshold.

The (N_A+1)-fold ionization of the initial atomic system is described by the electron-loss cross section

$$\sigma_L(N_A+1) = \sum_{nl} P(nl,N_A)\sigma(nl)\ , \tag{12}$$

where $P(nl,N_A)$ are the probabilities for the emission of N_A Auger electrons during the cascade decay process which follows the creation of a single nl-subshell vacancy. The single- and multiple-ionization cross sections resulting from single-electron ionization from the various nl subshells of argonlike Fe IX and neonlike Fe XVII ions by electron collisions are illustrated in Figs. 7 and 8, and the corresponding results which we have obtained for single-electron photoionization are displayed in Figs. 9 and 10. It can be seen that whereas the total multiple-ionization cross section never exceeds the single-ionization cross section for electron collisions, multiple ionization can be predominant during the cascade decay process which follows the K- and L-shell photoionization. This marked

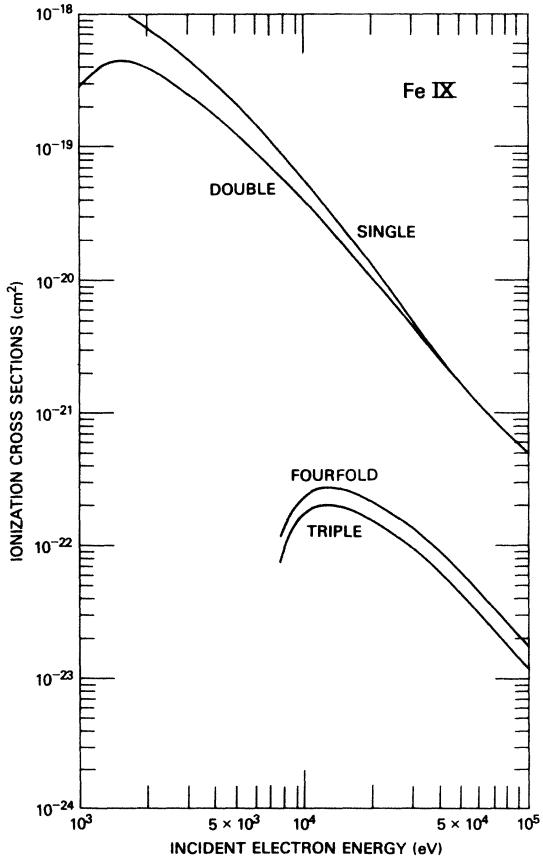

FIG. 7. The cross sections for single and multiple ionization during the vacancy-cascade decay process resulting from single-electron ionization from the various nl subshells or argonlike Fe IX ions by electron collisions, obtained from the evaluation of Eq. (12).

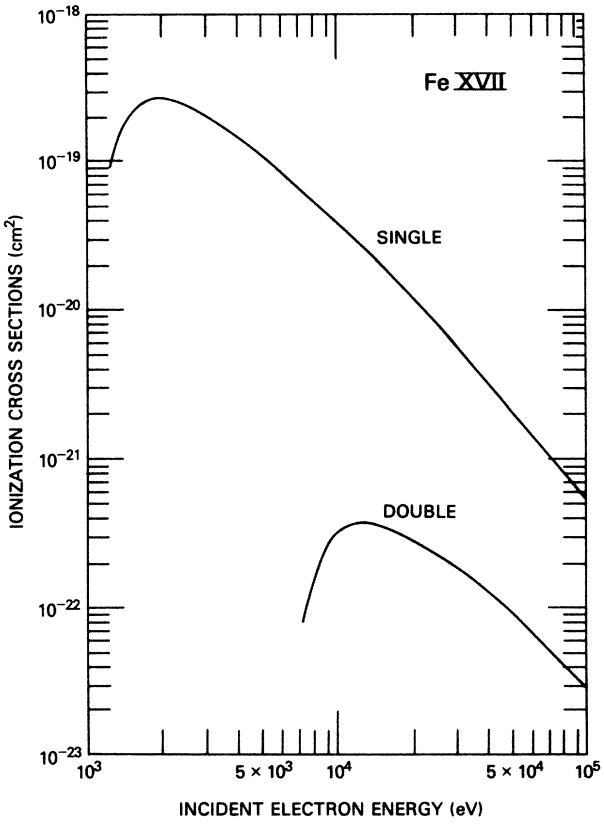

FIG. 8. The cross sections for single and multiple ionization during the vacancy-cascade decay process resulting from single-electron ionization from the various *nl* subshells of neonlike Fe XVII ions by electron collisions, obtained from the evaluation of Eq. (12).

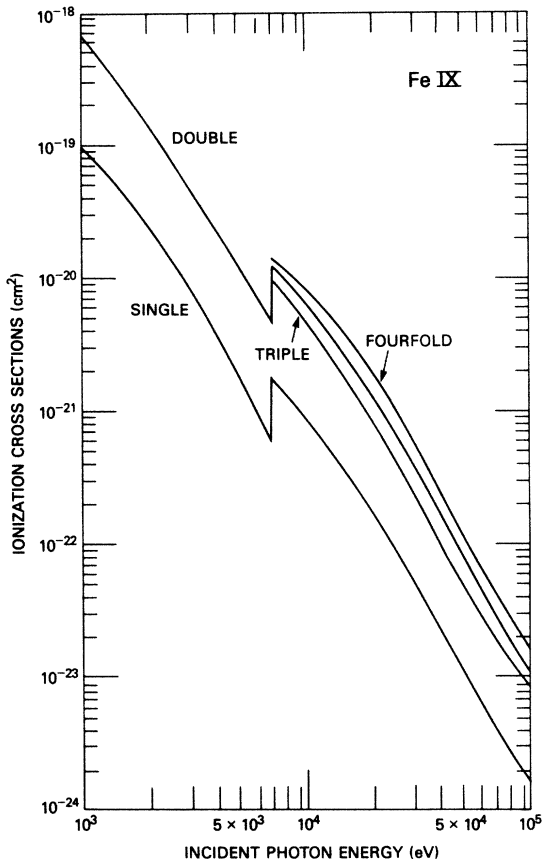

FIG. 9. The cross sections for single and multiple ionization during the vacancy-cascade decay process resulting from single-electron photoionization from the various *nl* subshells of argon-like Fe IX ions, obtained from the evaluation of Eq. (12).

difference in the importance of multiple ionization is directly attributable to the property that the most probable photoionization process involves the ejection of the most tightly bound *nl*-subshell electron that can be ionized at the particular incident photon energy.

V. CONCLUSIONS

We have developed an atomic inner-shell vacancy-cascade model by means of which a systematic determination can be made of the single- and multiple-ionization probabilities as well as of the characteristic x-ray line and the satellite line emission probabilities resulting from the sudden creation of an arbitrary distribution of inner-shell vacancies. We have applied our vacancy-cascade model to investigate the final products of single inner-shell-electron ionization of iron ions by electron collisions and by photon impacts. It has been concluded that single ionization and characteristic line emission are predominant during the vacancy-cascade decay process which follows the electron-collisional ionization of iron ions. However, the cascade decay process which follows the *K*-shell photoionization of iron ions can result predominantly in multiple ionization and can lead to the emission of satellite line radiation which is substantially more intense than the corresponding characteristic line radiation.

It is important to recognize the approximations which are inherent in our description of multiple ionization and photon emission accompanying the vacancy-cascade decay process which follows inner-shell-electron ionization. The fundamental assumption upon which our description has been based is that the vacancy-cascade process can be treated as a sequence of independent elementary Auger and radiative decay processes which occur subsequent to, and independent of, the sudden creation of a distribution of inner-shell vacancies. The frozen-core approximation, which has been employed in our calculation of the elementary decay rates, has restricted our treatment to the inclusion of only single-electron radiative transitions and Auger transitions which result in the creation of a single additional vacancy and in the emission of a single Auger electron. In the determination of the Auger and radiative decay rates for multiple-vacancy states, no attempt has been made to take into account the photon energy shifts or the energetic closing of the Coster-Kronig channels. Finally, we have ignored the effects of multiplet and fine structure, which have been found to be important in the

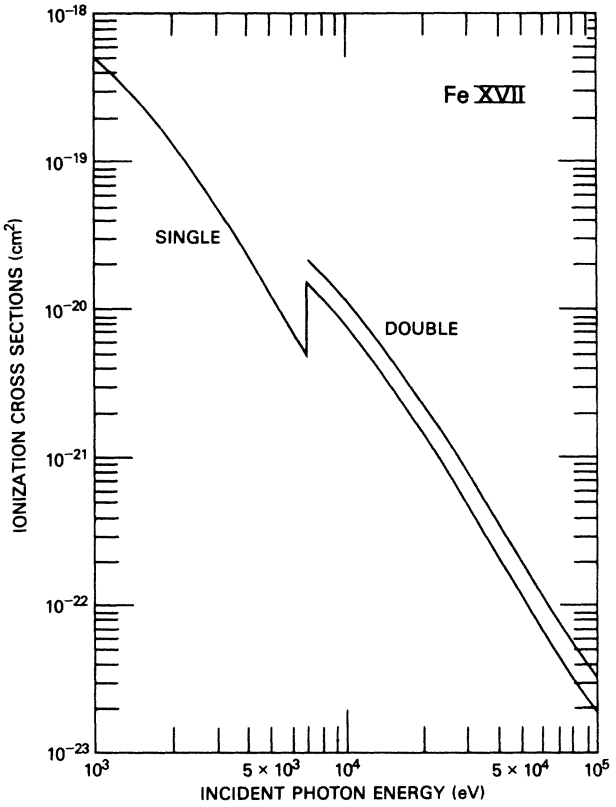

FIG. 10. The cross sections for single and multiple ionization during the vacancy-cascade decay process resulting from single-electron photoionization from the various *nl* subshells of neon-like Fe XVII ions, obtained from the evaluation of Eq. (12).

evaluation of Auger transition rates and fluorescence yields for highly charged ions.[22]

It is obvious that the multiple-ionization and photon-emission cross sections which have been introduced in this investigation strictly refer only to an isolated atomic system. The initial stages in the cascade decay of a deep inner-shell vacancy are expected to be essentially unaffected by the presence of surrounding atomic systems or charged particles. This is mainly a consequence of the fact that Auger transitions usually occur with the highest probability between neighboring shells. However, the final stages, in which a large number of vacancies are transferred to the outer shells, can be significantly affected by collision processes. It has been demonstrated[9] that the static screening produced by a high-density plasma can result in an energetic opening of the same Coster-Kronig channels which tend to close with increasing nuclear charge. This can have a significant effect on the distribution of final charge states and on the fluorescence probabilities.

ACKNOWLEDGMENTS

The authors wish to express their gratitude to John W. Cooper for his important contribution to the formulation of this description of the vacancy-cascade process and for numerous helpful discussions on the theory of atomic inner-shell processes. This work has been supported by the U.S. Office of Naval Research.

[1]H. R. Griem, *Plasma Spectroscopy* (McGraw-Hill, New York, 1964).
[2]D. P. Cox and W. H. Tucker, Astrophys. J. **157**, 1157 (1969).
[3]C. Jordan, Mon. Not. R. Astron. Soc. **142**, 501 (1969).
[4]V. L. Jacobs, J. Davis, P. C. Kepple, and M. Blaha, Astrophys. J. **211**, 605 (1977).
[5]S. Hatchett, J. Buff, and R. McCray, Astrophys. J. **206**, 847 (1976).
[6]J. C. Weisheit, Astrophys. J. **190**, 735 (1974).
[7]R. McCray, in *Galactic X-Ray Sources,* Proceedings of the NATO Advanced Study Institute, Cape Sounion, Greece, edited by P. Sanford (Wiley, New York, 1979).
[8]V. L. Jacobs, J. Davis, B. F. Rozsnyai, and J. W. Cooper, Phys. Rev. A **21**, 1917 (1980).
[9]B. R. Rozsnyai, V. L. Jacobs, and J. Davis, Phys. Rev. A **21**, 1798 (1980).
[10]E. P. Cooper, Phys. Rev. **61**, 1 (1942).
[11]T. A. Carlson and M. O. Krause, Phys. Rev. **137**, A1655 (1965).
[12]M. O. Krause and T. A. Carlson, Phys. Rev. **158**, 18 (1967).
[13]T. Aberg and G. Howat, in *Handbuch der Physik,* edited by W. Mehlhorn (Springer, Berlin, 1982), Vol. XXXI.
[14]L. Armstrong, Jr., C. E. Thedodosiou, and M. J. Wall, Phys. Rev. A **18**, 2538 (1978).
[15]S. L. Haan and J. Cooper, Phys. Rev. A **28**, 3349 (1983).
[16]V. L. Jacobs, Phys. Rev. A **31**, 383 (1985).
[17]T. Aberg, in *Atomic Inner-Shell Processes,* edited by B. Crasemann (Academic, New York, 1975), Vol. I.
[18]W. Bambynek, B. Crasemann, R. W. Fink, F. U. Freund, H. Mark, C. P. Swift, R. E. Price, and P. V. Rao, Rev. Mod. Phys. **44**, 716 (1972).
[19]D. L. Moores, L. B. Golden, and D. H. Sampson, J. Phys. B **13**, 385 (1980).
[20]D. H. Madison and E. Merzbacher, in *Atomic Inner-Shell Processes,* edited by B. Crasemann (Academic, New York, 1975), Vol. I.
[21]B. F. Rozsnyai and V. L. Jacobs (unpublished).
[22]M. H. Chen and B. Crasemann, Phys. Rev. A **12**, 959 (1975).